Letter

Direct evidence from high-field magnetotransport for a dramatic change of quasiparticle character in van der Waals ferromagnet $Fe_{3-x}GeTe_2$

S. Vaidya [1,*] M. J. Coak [1,2] D. A. Mayoh [1] M. R. Lees [1] G. Balakrishnan [1] J. Singleton [3] and P. A. Goddard [1,†]

[1]*Department of Physics, University of Warwick, Gibbet Hill Road, Coventry CV4 7AL, United Kingdom*

[2]*School of Physics & Astronomy, University of Birmingham, Edgbaston, Birmingham B15 2TT, United Kingdom*

[3]*National High Magnetic Field Laboratory (NHMFL), Los Alamos National Laboratory, Los Alamos, New Mexico 87545, USA*

(Received 21 December 2023; accepted 15 April 2024; published 10 July 2024)

Magnetometry and magnetoresistance (MR) data taken on the van der Waals ferromagnet $Fe_{3-x}GeTe_2$ (FGT) reveal three distinct contributions to the MR: a linear negative component, a contribution from closed Fermi-surface orbits, and an enhancement proportional to the square of the applied magnetic field which is linked to a noncoplanar spin arrangement. Contrary to earlier studies on FGT, by accounting for the field dependence of the anomalous Hall effect, we find that the ordinary Hall coefficient decreases markedly below 80 K, indicating a significant change in character of the electrons and holes on the Fermi-surface at this temperature. The resulting altered ground state eventually causes the Hall coefficient to reverse sign at 35 K. Our Hall data support the proposal that Kondo-lattice behavior develops in this d-electron material below 80 K. Additional evidence comes from the negative linear component of the MR, which arises from electron-magnon scattering with an atypical temperature dependence attributable to the onset of Kondo screening.

DOI: 10.1103/PhysRevResearch.6.L032008

Magnetic van der Waals (vdW) materials are emerging as an exciting testing ground for exploring fundamental theories of magnetism in the extreme two-dimensional (2D) limit [1–4], while the ease with which they can be exfoliated and reassembled into varied heterostructures makes them promising ingredients in devices that harness the interplay between magnetic moments and electronic transport properties [5,6]. Among these, the Fe-based compounds, such as $Fe_{3-x}GeTe_2$ (FGT) and Fe_3GaTe_2, have received significant attention due to their high Curie temperatures (T_C) and metallic behavior seldom seen in ferromagentic (FM) vdW materials. FGT in particular, with maximum reported T_C of 230 K [7], has been the subject of numerous studies exhibiting a wide range of phenomena, including topological nodal lines [8], a topological Hall effect [9,10], competing AFM fluctuations [11–13], and skyrmions [14].

The uniqueness of FGT in this regard has led to the development of multiple heterostructures that demonstrate potential for low-power spintronic technologies [15–17]. Nevertheless, consensus is yet to be reached on the fundamental magnetic and electronic processes that underpin these devices. The itinerant versus localized nature of the magnetism is of particular interest, and some recent angle-resolved photoemission spectroscopy (ARPES) and neutron-scattering studies suggest that FGT displays a coexistence of the two, with resulting Kondo-lattice behavior developing at low temperatures [13,18]. However, whilst Kondo-lattice behavior is widely accepted in f-electron systems, its presence in 3d compounds is more controversial [19,20]. While some degree of electronic correlation is known to exist in FGT (estimated quasiparticle effective masses range between 1.6 and 15.9 times the bare electron mass [18,21–24]), strong evidence for Kondo screening in the transport properties is so far elusive.

One reason that these issues remain unresolved is the paucity of high-quality transport data on samples close to the desired stoichiometry of Fe_3GeTe_2. The synthesis of this material has been shown from x-ray diffraction data to be challenging due to a propensity for vacancies on the Fe_I site (see Fig. 1). It is also known that these vacant sites lead to a reproducible suppression of the FM ordering from the ideal value of $T_C = 230$ K [26,27]. Several transport studies have been performed on samples exhibiting T_C less than 160 K [28–30], indicating that more than one in eight Fe ions are missing from the structure [27], with detrimental repercussions for the transport properties. Transport measurements on higher quality samples do exist [9,31], however, these papers overlook the significant field dependence of the factors contributing to the anomalous Hall effect (described below) when determining the behavior of the ordinary Hall coefficient. By performing magnetometry and magnetotransport measurements in high magnetic fields, we are able to take into account the presence of a nonsaturating magnetization, as well as the marked field dependence of the longitudinal magnetoresistance. In this way, we uncover evidence of multiple charge carrier types and a temperature-dependent evolution of the Fermi-surface (FS) properties that supports the Kondo-lattice scenario proposed [13,18] for FGT.

*s.vaidya@warwick.ac.uk

†p.goddard@warwick.ac.uk

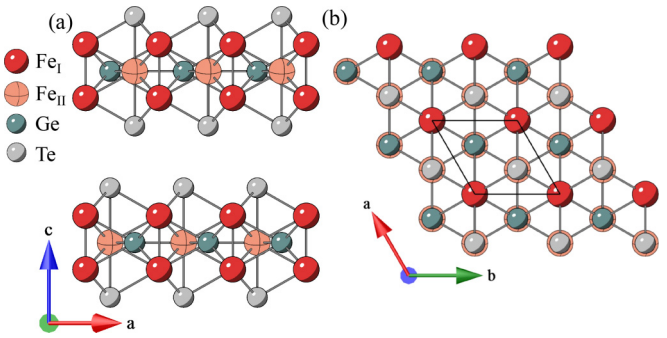

FIG. 1. Crystal structure (from data in Ref. [25]) of Fe_3GeTe_2 showing the Fe_I and Fe_{II} sites. View along (a) the *b* axis within the vdW-bonded layers, and (b) the *c* axis, perpendicular to the layers.

Large single crystals of FGT are grown using the chemical-vapour-transport method described in Ref. [27]. Bulk magnetometry measurements up to 9 T, are carried out using a vibrating sample magnetometer and measurements up to 7 T using a Magnetic Property Measurement System-XL SQUID magnetometer. Pulsed-field magnetization measurements are performed at the National High Magnetic Field Laboratory, Los Alamos, using several coaligned single crystals. Longitudinal transport and Hall effect measurements up to 9 T are carried out in a Quantum Design Physical Property Measurement System and high-field transport measurements are carried out at Los Alamos on flat-plate samples. Further experimental details including a discussion of demagnetization corrections are given in the Supplemental Material [32]. Field-cooled (FC) and zero-field-cooled (ZFC) temperature-dependent magnetic susceptibilities of FGT were measured with an applied field of $\mu_0 H = 0.01$ T and are shown in Fig. 2(a). A sharp deviation from Curie-Weiss behavior and bifurcation of the two curves indicate FM ordering at $T_C = 207(4)$ K. The suppression of T_C from 230 K suggests a Fe deficiency of $x \approx 0.15$ in the sample [27]. Energy-dispersive x-ray analysis confirms the sample composition to be $Fe_{2.90}GeTe_{2.12}$ [$x = 0.10(1)$], which is consistent with the ordering temperature and similar to the best samples for which

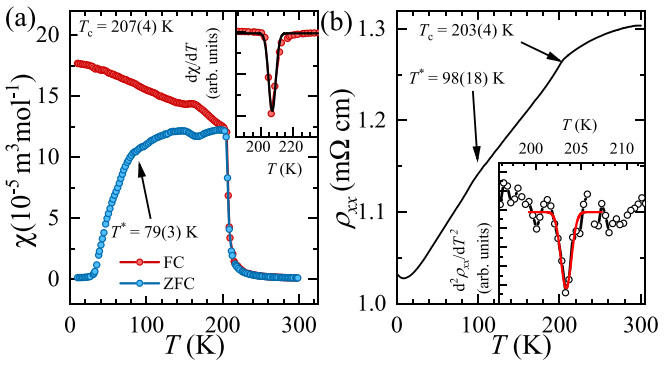

FIG. 2. (a) Zero-field-cooled (blue) and field-cooled (red) temperature-dependent magnetic susceptibility $\chi(T)$ for a single crystal of $Fe_{3-x}GeTe_2$, with a field of 0.01 T applied parallel to the *c* axis. Inset: A dip in $d\chi/dT$ indicates the ferromagnetic transition at T_C. (b) Temperature dependence of the in-plane resistivity ρ_{xx} in zero applied field. Inset: A dip in $d^2\rho_{xx}/dT^2$ occurs at T_C.

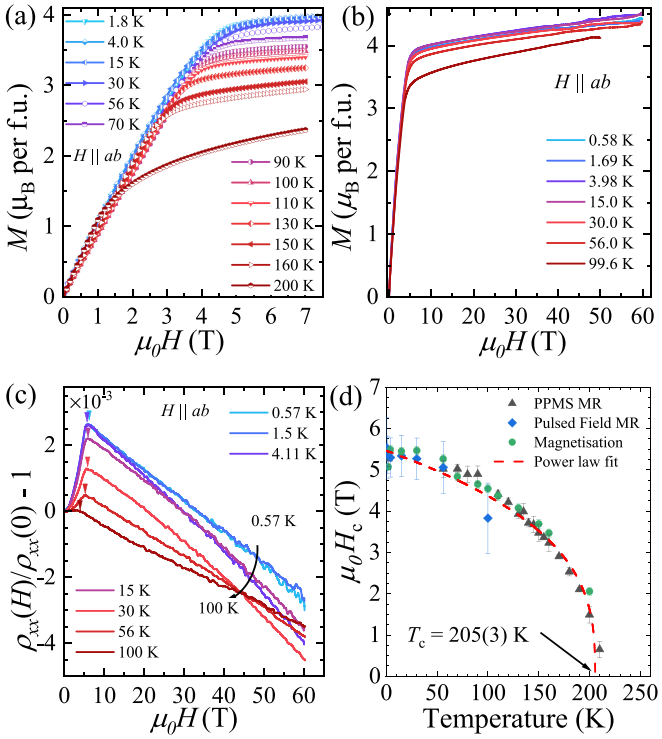

FIG. 3. Measurements with the applied field $H \parallel ab$. (a) Magnetization up to 7 T, (b) pulsed-field magnetization, and (c) longitudinal in-plane magnetoresistance. (d) $H_{ab} - T$ phase diagram. Black triangles and blue diamonds denote the H_c feature discussed in the text and marked by arrows in (c). Green circles mark the apparent saturation seen in the magnetization. Red dashed line is a fit to a power law described in the text.

transport and magnetometry data exist [9,10,31]. A kink is seen in both the FC and ZFC curves at $T = 161(1)$ K, consistent with previous reports of possible AFM fluctuations [11]. Furthermore, there is a sudden drop in the ZFC on cooling data at $T^* = 79(3)$ K.

Figure 2(b) displays the temperature dependence of the in-plane longitudinal resistivity, ρ_{xx}. The curves exhibit metallic behavior with a sharp change in gradient, observed as a minimum in $d^2\rho_{xx}/dT^2$, associated with the FM ordering at $T_C = 203(4)$ K. This is in agreement with the $\chi(T)$ data. An additional change in the gradient is observed at $T^* = 98(18)$ K, prior to an upturn below $T = 8.0(3)$ K. The characteristic temperature T^* has previously been suggested to signify the onset of Kondo-lattice behavior in FGT [13,18].

Figures 3(a) and 3(b) present the isothermal magnetization M at various temperatures as a function of $H \parallel ab$. $M(H)$ rises quickly at low fields to an apparent saturation, which is followed by a much slower increase up to 60 T, which could be due to the movement of domain walls stuck on strong pinning sites or exchange-enhanced Pauli paramagnetism, as seen in other ferromagnetic metals [33,34].

The longitudinal in-plane magnetoresistance (MR) with $H \parallel ab$ (with an in-plane current $I \perp H$) is displayed in Fig. 3(c). At low fields and low temperatures, the MR increases $\propto H^2$ before reversing gradient abruptly at H_c. By 80 K, the low-field H^2 dependence of the MR is no longer present; however, a shoulder feature at H_c persists up to T_c as

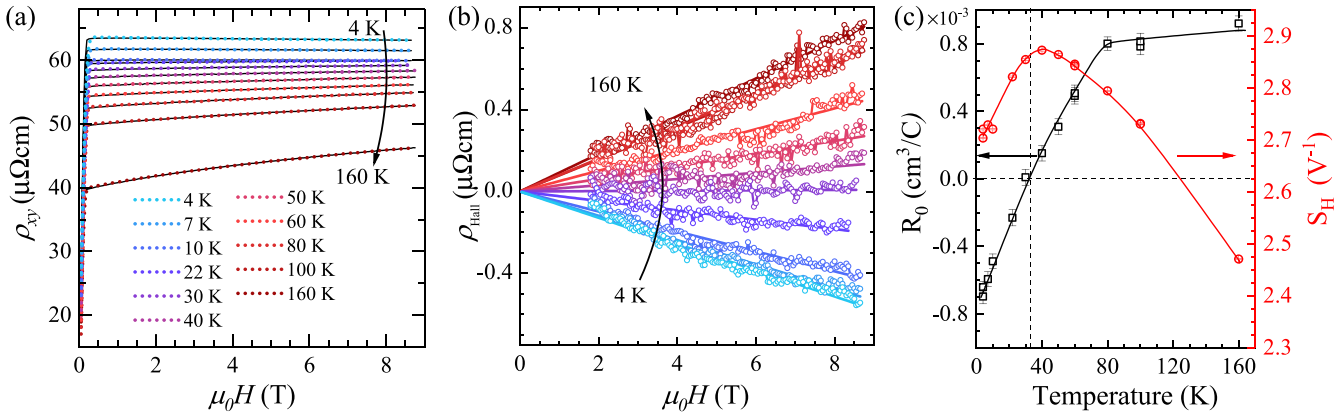

FIG. 4. (a) The in-plane Hall resistivity ρ_{xy} (small circles) as a function of $H \parallel c$ at all temperatures measured are in excellent agreement with (and hence lie underneath) the results of the fits described in the text (solid lines). For clarity, the curves have been offset by 2 $\mu\Omega$cm. (b) The ordinary Hall effect component $\rho_{\rm Hall}$ extracted from the fitting process. (c) Temperature dependence of the ordinary Hall coefficient R_0 (black squares) and the AHE scale factor S_H (red circles). Solid lines are a guide to the eye.

shown in the Supplemental Material [32]. Figure 3(d) shows the result of plotting H_c as a function of temperature alongside the apparent saturation field seen in the $M(H \parallel ab)$ data. It can be seen that the feature found in the transport measurement maps out the same phase boundary seen in the in-plane magnetometry. A power-law fit of the form $H_c = H_0(1 - T/T_c)^\delta$ yields $\mu_0 H_0 = 5.46(7)$ T, $\delta = 0.33(2)$, and $T_C = 205(3)$ K, in excellent agreement with the FM ordering temperature determined earlier. A similar phase boundary has previously been mapped through observations of the topological Hall effect, which arises due to the noncoplanar spin configuration that exists for $H \parallel ab$ below the saturation field [9,10,29]. However, an enhancement of the longitudinal MR associated with the canted phase was not seen in those studies (likely for the reasons discussed earlier). We note that the MR behavior is symmetric in field and so does not arise from a poor subtraction of the Hall component of the resistivity [32]. Nevertheless, quite why the MR would show a H^2 increase within the noncoplanar magnetic phase remains to be explained.

Figure 4(a) shows the Hall resistivity ρ_{xy} measured with $I \parallel ab$ and $H \parallel c$. Typically in FM conductors, the Hall effect is composed of two components

$$\rho_{xy} = \rho_{\rm Hall} + \rho_{\rm AH} = R_0\mu_0 H + \mu_0 R_S M, \quad (1)$$

where the $\rho_{\rm Hall}$ is the ordinary Hall effect with coefficient R_0 and $\rho_{\rm AH}$ is the anomalous Hall effect (AHE) with coefficient R_S. Previous studies have shown that the Karplus-Luttinger mechanism, with $R_S \propto \rho_{xx}^2$, is dominant in FGT [8,9,31,35]. Consequently, the Hall resistivity can be written as

$$\rho_{xy} = R_0\mu_0 H + S_H\rho_{xx}^2 M, \quad (2)$$

where S_H is the AHE scaling factor. In this equation, the field-dependence of both M and ρ_{xx} is neglected in earlier reports on FGT [9,31]. Our data show that these contributions to the AHE are not insignificant (as previously assumed) and must be taken into account to achieve a reliable analysis of the Hall data. (In the Supplemental Material, we use the previously reported analysis method on our Hall data and show that it leads to erroneous conclusions regarding the nature of the charge carriers.) Figures 5(a) and 5(b), respectively, show the results of our measurements of these quantities for $H \parallel c$. Similar to the case for an in-plane field, the $M(H)$ data with $H \parallel c$ display a sharp rise to an apparent saturation, but then continue to increase more gradually up to 60 T.

The MR data in Fig. 5(b) exhibits a strong negative trend up to the highest fields. Our data show that these contributions to the AHE are not insignificant and must be taken into account to achieve a reliable analysis of the Hall data. If this is done, then the parameters S_H and R_0 in Eq. (2) can be extracted from linear fits to $\rho_{xy}/\mu_0 H$ vs $\rho_{xx}^2 M/\mu_0 H$, at $\mu_0 H \geqslant 2$ T. The parameters extracted in this way can be inserted back into Eq. (2) as a check, and the calculated ρ_{xy} is seen to be in excellent agreement with the raw data [see solid lines in Fig. 4(a)]. Moreover, the isolated $\rho_{\rm Hall}$ component is shown in Fig. 4(b) and is found to be linear in H at all temperatures, as expected.

The temperature dependence of the extracted R_0 and S_H parameters are shown in Fig. 4(c). Between 160 and 80 K, R_0 is roughly constant and positive, indicating the presence of dominant hole carriers. On cooling further, the Hall coefficient drops steadily, becoming negative for $T \lesssim 35$ K. S_H exhibits a maximum at around the same temperature. The behavior of $R_0(T)$ clearly confirms the presence of both electron and hole pockets in the FS of FGT, as suggested by previous ARPES measurements [18,22].

The sudden drop in $R_0(T)$ at around 80 K implies that a significant change in the FS takes place at this temperature. A previous report comparing neutron scattering and dynamical mean-field theory suggested that an orbitally selective Mott transition occurs at $T \approx 100$ K [12], which would indeed result in a marked change in R_0. However, the transition predicted in Ref. [12] would lead to a loss of an electron pocket at the K point. By contrast, our results suggest that a significant increase in electron density and/or mobility (relative to the holes) sets in at 80 K [36]. On the other hand, the abrupt drop in R_0 occurs very close to the features we observe in $\chi(T)$ and ρ_{xx} at $T^* = 80$ K, and which have been seen by other authors [11,13,18]. Using evidence from ARPES, STM, and neutron spectroscopy, Refs. [18] and [13] suggest that T^* marks the onset temperature of Kondo-lattice behavior, below which

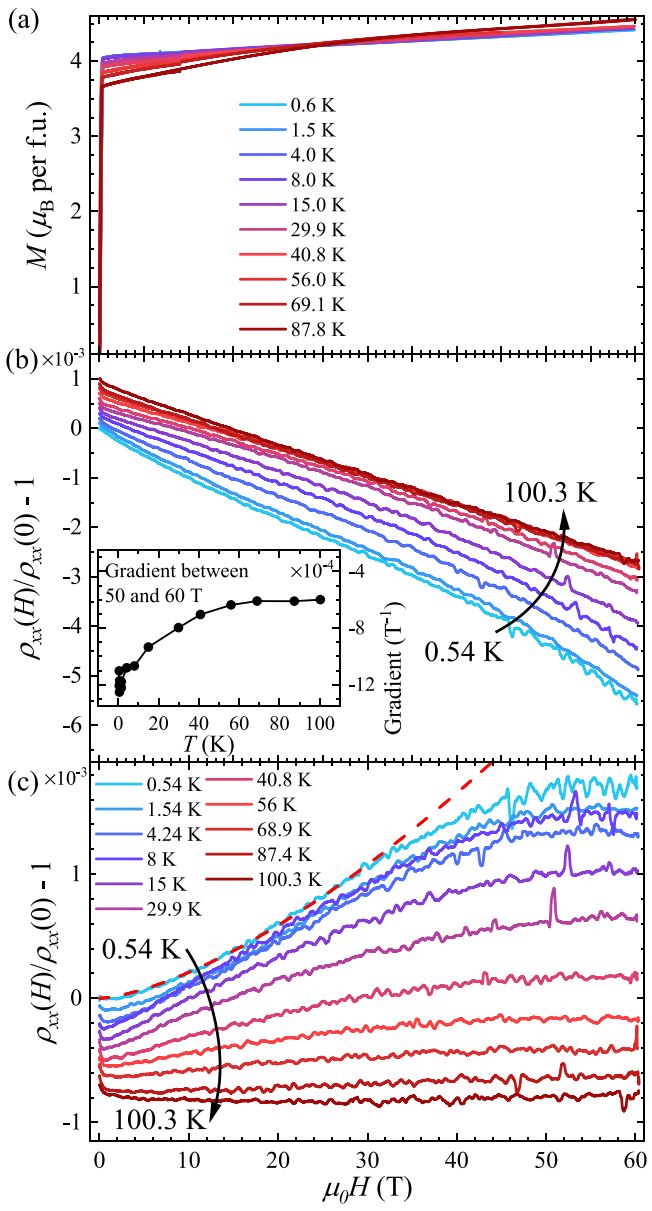

FIG. 5. Measurements with $H \parallel c$. (a) Magnetization up to 60 T. (b) In-plane magnetoresistance (MR). An offset of 0.1% has been applied for clarity. Inset: Gradient of the negative linear component. (c) MR after the linear component has been removed (curves offset for clarity). The red dashed line shows an $H^{1.5}$ fit to the 0.54 K data.

coherent heavy quasiparticles emerge and act to screen the local moments, as is seen in f-electron heavy-fermion materials. The resulting alteration in the FS properties would readily explain the drop we see in the Hall coefficient below T^*.

Further support for the Kondo-lattice picture comes from the $H \parallel c$ MR data shown in Fig. 5(b), which exhibits a strong negative trend for all temperatures up to 60 T [similar to the in-plane field data above H_c, see Fig. 3(c)]. The absence of the low-field H^2 dependence in the $H \parallel c$ MR data confirms that that behavior is indeed connected to the canted magnetic phase which only exists for in-plane fields. For the $H \parallel c$ data, the MR is dominated by a negative linear component, with a smaller additional dependence apparent at low temperatures and fields. Fitting the MR between 50 and 60 T to obtain the negative linear component and subtracting it from the data yields a positive, saturating component that diminishes as temperature is raised and disappears completely close to 100 K, as shown in Fig. 5(c).

Positive MR is typically caused by the orbital motion of charge carriers on a nonspherical FS. A simple closed FS pocket is expected to produce a saturating MR with a H^2 dependence at low-fields, while a nonsaturating MR arises from either open FS orbits or perfect charge compensation in a simple two-band model (see, e.g., Ref. [37]). In our data at 0.54 K, the MR below 30 T can be described by MR $\propto H^\delta$, with $\delta = 1.5(1)$, before saturating at $\mu_0 H \approx 50$ T. Such behavior is consistent with the presence of different carrier types on multiple closed FS pockets and a marked deviation from charge compensation, a situation that is in agreement with the R_0 data presented earlier. It is also in keeping with prior theoretical and experimental work on FGT, which consistently reveals multiple closed orbits within the k_x-k_y plane [12,18,24].

As mentioned, at all temperatures measured, the MR is dominated by a negative linear component. Such a response is well established in FMs as the result of a reduction in electron-magnon scattering caused by the damping of spin waves with applied field [38], a situation that has been suggested for FGT previously [30,31]. Typically, because the magnon population diminishes at low temperatures (where it is harder to flip a spin), the strength of the negative MR is found to decrease on cooling [38]. However, the situation in FGT might be expected to be different. The inelastic neutron scattering data presented in Ref. [13] show that, in a departure from the typical behavior of spin waves, the low-energy magnons in FGT are more coherent at elevated temperatures, a result that is attributed to enhanced Kondo screening of local moments as the temperature is reduced below T^*. As a result, one might expect that the additional damping caused by an applied magnetic field would have a larger effect on electron-magnon scattering as the temperature is reduced, than at high temperatures where the lifetime and coherence of the spin waves are enhanced. Accordingly, we find that the negative MR gradient in FGT begins to increase as the temperature is reduced below 70 K [see Fig. 3(b)], which is close to the $T^* \approx 80$ K value seen in our measurements of $\chi(T)$, $\rho_{xx}(T)$, and $R_0(T)$.

Taken together, our data paint a consistent picture of a clear change in the character (i.e., effective mass, scattering rates and possibly relative numbers) of the electrons and/or holes at the FS, caused by the onset of Kondo-lattice physics. Our results establish a connection between the transport properties and the earlier results of ARPES and neutron spectroscopy highlighting the heavy-fermion-like properties of FGT. The interplay of localized and itinerant magnetism, common in f-electron materials, is still an unusual proposition in transition-metal systems and warrants further investigation using other FS-sensitive probes.

Data presented in this paper will be made available [39].

This project has received funding from the European Research Council (ERC) under the European Union's Horizon 2020 research and innovation programme (Grant Agreement

No. 681260) and the UK Engineering and Physical Sciences Research Council (EPSRC) (Grants No. EP/T005963/1 and No. EP/N032128/1). A portion of this work was performed at the National High Magnetic Field Laboratory (NHMFL), which is supported by National Science Foundation Cooperative Agreements No. DMR-1644779 and No. DMR-2128556, and the Department of Energy (DOE). J.S. acknowledges support from the DOE BES program "Science at 100 T," which permitted the design and construction of much of the specialized equipment used in the high-field studies.

[1] P. Ajayan, P. Kim, and K. Banerjee, Two-dimensional van der Waals materials, Phys. Today **69**, 38 (2016).

[2] K. S. Burch, D. Mandrus, and J.-G. Park, Magnetism in two-dimensional van der Waals materials, Nature (London) **563**, 47 (2018).

[3] Y. Khan, S. M. Obaidulla, M. R. Habib, A. Gayen, T. Liang, X. Wang, and M. Xu, Recent breakthroughs in two-dimensional van der Waals magnetic materials and emerging applications, Nano Today **34**, 100902 (2020).

[4] Q. H. Wang, A. Bedoya-Pinto, M. Blei, A. H. Dismukes, A. Hamo, S. Jenkins, M. Koperski, Y. Liu, Q.-C. Sun, E. J. Telford *et al.*, The magnetic genome of two-dimensional van der Waals materials, ACS Nano **16**, 6960 (2022).

[5] S.-J. Liang, B. Cheng, X. Cui, and F. Miao, Van der Waals heterostructures for high-performance device applications: Challenges and opportunities, Adv. Mater. **32**, 1903800 (2020).

[6] J. F. Sierra, J. Fabian, R. K. Kawakami, S. Roche, and S. O. Valenzuela, Van der Waals heterostructures for spintronics and opto-spintronics, Nat. Nanotechnol. **16**, 856 (2021).

[7] H.-J. Deiseroth, K. Aleksandrov, C. Reiner, L. Kienle, and R. K. Kremer, Fe_3GeTe_2 and Ni_3GeTe_2–two new layered transition-metal compounds: Crystal structures, HRTEM investigations, and magnetic and electrical properties, Eur. J. Inorg. Chem. **2006**, 1561 (2006).

[8] K. Kim, J. Seo, E. Lee, K.-T. Ko, B. Kim, B. G. Jang, J. M. Ok, J. Lee, Y. J. Jo, W. Kang *et al.*, Large anomalous Hall current induced by topological nodal lines in a ferromagnetic van der Waals semimetal, Nat. Mater. **17**, 794 (2018).

[9] Y. Wang, C. Xian, J. Wang, B. Liu, L. Ling, L. Zhang, L. Cao, Z. Qu, and Y. Xiong, Anisotropic anomalous Hall effect in triangular itinerant ferromagnet Fe_3GeTe_2, Phys. Rev. B **96**, 134428 (2017).

[10] R. R. Chowdhury, S. DuttaGupta, C. Patra, O. A. Tretiakov, S. Sharma, S. Fukami, H. Ohno, and R. P. Singh, Unconventional Hall effect and its variation with Co-doping in van der Waals Fe_3GeTe_2, Sci. Rep. **11**, 14121 (2021).

[11] J. Yi, H. Zhuang, Q. Zou, Z. Wu, G. Cao, S. Tang, S. Calder, P. Kent, D. Mandrus, and Z. Gai, Competing antiferromagnetism in a quasi-2D itinerant ferromagnet: Fe_3GeTe_2, 2D Mater. **4**, 011005 (2016).

[12] X. Bai, F. Lechermann, Y. Liu, Y. Cheng, A. I. Kolesnikov, F. Ye, T. J. Williams, S. Chi, T. Hong, G. E. Granroth *et al.*, Antiferromagnetic fluctuations and orbital-selective Mott transition in the van der Waals ferromagnet $Fe_{3-x}GeTe_2$, Phys. Rev. B **106**, L180409 (2022).

[13] S. Bao, W. Wang, Y. Shangguan, Z. Cai, Z.-Y. Dong, Z. Huang, W. Si, Z. Ma, R. Kajimoto, K. Ikeuchi, S.-I. Yano, S.-L. Yu, X. Wan, J.-X. Li, and J. Wen, Neutron spectroscopy evidence on the dual nature of magnetic excitations in a van der Waals metallic ferromagnet $Fe_{2.72}GeTe_2$, Phys. Rev. X **12**, 011022 (2022).

[14] Y. Li, R. Basnet, K. Pandey, J. Hu, W. Wang, X. Ma, A. R. C. McCray, A. K. Petford-Long, and C. Phatak, Field-dependent magnetic domain behavior in van der Waals Fe_3GeTe_2, JOM **74**, 2310 (2022).

[15] S. Albarakati, C. Tan, Z.-J. Chen, J. G. Partridge, G. Zheng, L. Farrar, E. L. Mayes, M. R. Field, C. Lee, Y. Wang *et al.*, Antisymmetric magnetoresistance in van der Waals Fe_3GeTe_2/graphite/Fe_3GeTe_2 trilayer heterostructures, Sci. Adv. **5**, eaaw0409 (2019).

[16] Y. Wu, S. Zhang, J. Zhang, W. Wang, Y. L. Zhu, J. Hu, G. Yin, K. Wong, C. Fang, C. Wan *et al.*, Néel-type skyrmion in WTe_2/Fe_3GeTe_2 van der Waals heterostructure, Nat. Commun. **11**, 3860 (2020).

[17] Y. Wu, B. Francisco, Z. Chen, W. Wang, Y. Zhang, C. Wan, X. Han, H. Chi, Y. Hou, A. Lodesani *et al.*, A van der Waals interface hosting two groups of magnetic skyrmions, Adv. Mater. **34**, 2110583 (2022).

[18] Y. Zhang, H. Lu, X. Zhu, S. Tan, W. Feng, Q. Liu, W. Zhang, Q. Chen, Y. Liu, X. Luo, D. Xie, L. Luo, Z. Zhang, and X. Lai, Emergence of Kondo lattice behavior in a van der Waals itinerant ferromagnet, Fe_3GeTe_2, Sci. Adv. **4**, eaao6791 (2018).

[19] H. Liu, Y. Cao, Y. Xu, D. J. Gawryluk, E. Pomjakushina, S.-Y. Gao, P. Dudin, M. Shi, L. Yan, Y.-F. Yang, and H. Ding, Observation of flat bands due to band hybridization in the 3*d*-electron heavy-fermion compound $CaCu_3Ru_4O_{12}$, Phys. Rev. B **102**, 035111 (2020).

[20] Y.-f. Yang, An emerging global picture of heavy fermion physics, J. Phys.: Condens. Matter **35**, 103002 (2022).

[21] J.-X. Zhu, M. Janoschek, D. S. Chaves, J. C. Cezar, T. Durakiewicz, F. Ronning, Y. Sassa, M. Mansson, B. L. Scott, N. Wakeham, E. D. Bauer, and J. D. Thompson, Electronic correlation and magnetism in the ferromagnetic metal Fe_3GeTe_2, Phys. Rev. B **93**, 144404 (2016).

[22] X. Xu, Y. W. Li, S. R. Duan, S. L. Zhang, Y. J. Chen, L. Kang, A. J. Liang, C. Chen, W. Xia, Y. Xu, P. Malinowski, X. D. Xu, J. H. Chu, G. Li, Y. F. Guo, Z. K. Liu, L. X. Yang, and Y. L. Chen, Signature for non-Stoner ferromagnetism in the van der Waals ferromagnet Fe_3GeTe_2, Phys. Rev. B **101**, 201104(R) (2020).

[23] Y. Sun, J. Zhang, T. Yao, X. F. Sun, S.-h. Ke, J. Zhang, and S. M. Zhou, Kadowaki-Woods relation and thermal transport in the two-dimensional van der Waals ferromagnet Fe_3GeTe_2, Phys. Rev. B **107**, 094416 (2023).

[24] C. Trainer, O. R. Armitage, H. Lane, L. C. Rhodes, E. Chan, I. Benedičič, J. A. Rodriguez-Rivera, O. Fabelo, C. Stock, and P. Wahl, Relating spin-polarized STM imaging and inelastic neutron scattering in the van der Waals ferromagnet Fe_3GeTe_2, Phys. Rev. B **106**, L081405 (2022).

[25] Fe_3GeTe_2 crystal structure: datasheet from PAULING FILE Multinaries Edition–2022 in *Springer Materials* (available at: https://materials.springer.com/isp/crystallographic/docs/sd_1420956)

[26] A. F. May, S. Calder, C. Cantoni, H. Cao, and M. A. McGuire, Magnetic structure and phase stability of the van der Waals bonded ferromagnet $Fe_{3-x}GeTe_2$, Phys. Rev. B **93**, 014411 (2016).

[27] D. A. Mayoh, G. D. A. Wood, S. J. R. Holt, G. Beckett, E. J. L. Dekker, M. R. Lees, and G. Balakrishnan, Effects of Fe deficiency and Co substitution in polycrystalline and single crystals of Fe_3GeTe_2, Cryst. Growth Des. **21**, 6786 (2021).

[28] Y. Liu, E. Stavitski, K. Attenkofer, C. Petrovic *et al.*, Anomalous Hall effect in the van der Waals bonded ferromagnet $Fe_{3-x}GeTe_2$, Phys. Rev. B **97**, 165415 (2018).

[29] Y. You, Y. Gong, H. Li, Z. Li, M. Zhu, J. Tang, E. Liu, Y. Yao, G. Xu, F. Xu, and W. Wang, Angular dependence of the topological Hall effect in the uniaxial van der Waals ferromagnet Fe_3GeTe_2, Phys. Rev. B **100**, 134441 (2019).

[30] J. Ke, M. Yang, W. Xia, H. Zhu, C. Liu, R. Chen, C. Dong, W. Liu, M. Shi, Y. Guo, and J. Wang, Magnetic and magnetotransport studies of two-dimensional ferromagnetic compound Fe_3GeTe_2, J. Phys.: Condens. Matter **32**, 405805 (2020).

[31] P. Saha, M. Singh, V. Nagpal, P. Das, and S. Patnaik, Scaling analysis of anomalous Hall resistivity and magnetoresistance in the quasi-two-dimensional ferromagnet Fe_3GeTe_2, Phys. Rev. B **107**, 035115 (2023).

[32] See Supplemental Material at http://link.aps.org/supplemental/10.1103/PhysRevResearch.6.L032008 for experimental details, further analysis of the Hall effect and rotation dependent magnetoresistance data.

[33] A. Freeman, N. Blum, S. Foner, R. B. Frankel, and E. McNiff, Jr., Ferromagnetic metals in high magnetic fields, J. Appl. Phys. **37**, 1338 (1966).

[34] C. Herring, R. Bozorth, A. Clark, and T. McGuire, High-field susceptibilities of iron and nickel, J. Appl. Phys. **37**, 1340 (1966).

[35] J. Xu, W. A. Phelan, and C.-L. Chien, Large anomalous Nernst effect in a van der Waals ferromagnet Fe_3GeTe_2, Nano Lett. **19**, 8250 (2019).

[36] To put it another way, a significant decrease in the density and/or mobility of the holes, relative to those of the electrons, sets in at 80 K.

[37] S. N. Zhang, Q. S. Wu, Y. Liu, and O. V. Yazyev, Magnetoresistance from Fermi surface topology, Phys. Rev. B **99**, 035142 (2019).

[38] B. Raquet, M. Viret, E. Sondergard, O. Cespedes, and R. Mamy, Electron-magnon scattering and magnetic resistivity in 3*d* ferromagnets, Phys. Rev. B **66**, 024433 (2002).

[39] wrap.warwick.ac.uk/185005/.